CLOUD AND RADIATIVE FIELDS DERIVED FROM GOES-8 DURING SUCCESS AND THE ARM-UAV SPRING 1996 FLIGHT SERIES

Patrick Minnis
Atmospheric Sciences Division
NASA Langley Research Center
Hampton, Virginia 23681

William L. Smith, Jr.
Analytical Services and Materials, Inc.
Hampton, Virginia 23666

Submitted to *Geophysical Research Letters* SUCCESS Special Issue
June 1997

Abstract. Cloud and radiative properties were derived for the southern Great Plains for April 9 - May 9, 1996 from GOES-8 to provide a large-scale context for SUCCESS and a dataset for mesoscale modeling of cirrus processes. The analyses indicate that cloudiness over the domain was below normal during April 1996. Thin cirrus with optical depths less than 6 was the predominant cloud type over much of the domain, however, providing a considerable number of measurement opportunities for the suite of SUCCESS instruments. Diurnal variation of cloudiness was substantial over the ARM southern Great Plains central facility. Total albedos were below normal because of the diminished cloudiness, while surface temperature and total longwave fluxes were relatively high. The data are on a 0.5° grid and are available electronically.

Introduction

The Subsonic Clouds and Contrails Effects Special Study (SUCCESS) experiment conducted during the spring of 1996 took measurements primarily over the southern Great Plains (SGP). Observations from surface, aircraft, and satellites comprise the SUCCESS data. Surface measurements were concentrated at the Atmospheric Radiation Measurement (ARM) Program (Stokes and Schwartz (1994) SGP Central Facility (SCF) near LaMont, Oklahoma, while most of the aircraft data were acquired over various locations in Oklahoma, Kansas, and Colorado, including the SCF. Other aircraft measurements were also obtained over the SCF as part of the ARM Unmanned Aerospace Vehicle (UAV) Program Spring 1996 Flight Series. Satellite observations provide the large-scale perspective that complements the spatially limited surface data and temporally constrained aircraft measurements. Relatively low-resolution satellite data can be used to derive bulk cloud properties and top-of-the-atmosphere (TOA) broadband radiative fluxes important for a variety of applications. This paper provides a summary of the satellite-derived mesoscale cloud and radiative environment during SUCCESS to understand the large-scale context for the other SUCCESS and ARM UAV observations, to document a dataset useful for testing cloud process models and algorithm verification, and to determine the cloud radiative forcing during the experiment.

Data and Methodology

Half-hourly, 4-km Geostationary Operational Environmental Satellite (GOES-8) visible (VIS; 0.65 μm) and infrared (IR; 10.9 μm) radiances were analyzed with the layer bispectral threshold method (LBTM) of Minnis et al. (1995) to estimate cloud fraction C, optical depth τ, center and top temperatures T_c and T_t, and center and top heights z_c and z_t during the daytime for solar zenith angles $\theta_o < 78°$. At all other times, an infrared-only method was used to estimate C, T_c, and z_c using the assumption that all of the clouds are optically thick. The LBTM cloud amounts are based on the fraction of pixels having IR temperatures $T < T_{cs}$ - 6.5K or VIS reflectance $\rho > \rho_{cs} + \Delta\rho$, where $\Delta\rho$ is the clear-sky tolerance as defined by Minnis et al. (1995) and the subscript cs refers to clear-sky values. The cloud properties are determined for each grid box and time in three layers: low, middle, and high with altitude boundaries $z < 2$ km, $2 \le z < 6$ km, and $z > 6$ km, respectively. Optical depth is derived for low and midlevel clouds using a reflectance model that assumes water droplets having an effective radius of 10 μm. High cloud optical depths are based on a cirrostratus cloud having idealized randomly oriented, hexagonal ice columns with an effective diameter of ~ 41 μm (Minnis et al., 1993). If a value for τ is available, an IR emittance is computed and the observed IR temperature is adjusted to determine T_c when the cloudy pixel is semitransparent. An additional adjustment is applied to estimate T_t for optically thin clouds. The values of T_c and T_t are identical when the cloud is optically thick. If τ is unavailable, $T_c = T$. Thus, when $\theta_o < 78°$, the temperatures and heights for optically thin clouds will be over- and underestimated, respectively.

The cloud parameters were derived for a 0.5° x 0.5° grid between 32°N and 42°N and 91°W and 105°W for April 9 - May 9, 1996. This domain includes most of the SUCCESS aircraft flights. An analysis was also performed using a nine-region, 0.3° x 0.3° grid centered on the SCF

(36.48°N, 97.5°W) to provide higher resolution data for direct comparison with the SCF instruments. The VIS count data were converted to reflectances using the formula,

$$\rho = \frac{\pi L_V}{526.9 \cos\theta_o \, \delta(D)}, \quad (1)$$

where $L_v = 0.691\ CT - 19.4$ (Minnis et al., 1997), CT is the 10-bit count, D is the day of the year, and δ is the Earth-Sun distance correction factor. The nominal GOES-8 calibration was used to convert counts to IR temperatures. Soundings from National Weather Service stations surrounding and within the large domain were interpolated to obtain temperature and relative humidity profiles at each time step and grid box. These profiles were used to convert temperature to altitude.

The VIS reflectances and IR temperatures were converted to VIS albedo α_v and IR flux M_{ir}, respectively, as in Minnis et al. (1995). These values were then converted to shortwave (SW; 0.2 - 5.0 μm) albedo α_{sw} and longwave (LW; 5 - 50 μm) flux M_{lw} using empirical relationships based on correlations between coincident October 1986 GOES-6 and Earth Radiation Budget Experiment satellite data (Minnis et al., 1997b). These conversion formulae are

$$\alpha_{sw} = 0.057 + 0.720\ \alpha_v + 0.0287\ \alpha_v^{\,2} + 0.023 \ln(1/\cos\theta_o), \quad (2)$$

and

$$M_{lw} = 77.2 + 5.55 M_{ir} - 0.0171\ M_{ir}^2 - 0.237\ M_{ir} \ln(RH), \quad (3)$$

here RH is the mean relative humidity for all layers above the altitude $z(T_m)$, where T_m is the mean IR temperature in the grid box. Shortwave and longwave cloud forcing SWCF and LWCF, respectively, are computed as in Ramanathan et al. (1989).

Results

Figure 1 shows an example of the time series of cloud amounts and optical depths for the 0.3° box centered at the SCF for April 20 and 21, two days when the NASA DC-8 flew several flight patterns over the SCF. April 20 started clear with a rapid increase in cloudiness that consisted primarily of thin high clouds with z_c = 12 km gradually decreasing to 4 km for total cloudiness by the end of the day. At 2345 UTC, C(high) = 4% at 7 km. Optical depth was less than unity until ~1500 UTC. It then varied from 0.6 and 2.2 during the remainder of April 20. The cirrus came in waves during April 21 with z_c fluctuating between 5 and 10 km until the end of the day when a cumulonimbus developed increasing τ from values of 1 -3 up to 30 - 70. The anvil cloud reached an altitude of 14 km. Nocturnal clouds are not shown because optical depth is unavailable.

The mean diurnal cycles of cloud and radiative properties for the SCF 0.3° box are presented in Figure 2. Total cloud cover (Figure 2a) peaks around sunset at ~1800 Local Time (LT) with a secondary maximum near 0900 LT. A distinct minimum in cloudiness occurs before midnight when virtually no high or low clouds were detected. This minimum corresponds to relative maximum in M_{lw} (Figure 2d) that nearly matches the daytime peak of 262 Wm^{-2}. High clouds appear to peak at 1000 and 1700 LT, while the midlevel clouds reach a maximum at 1900 LT. With no correction for semitransparency after 1730 LT, some of the midlevel clouds may actually be high clouds at 1900 LT. The relative maximum in C(total) at sunrise is accompanied by large optical depths (Figure 2c) and a pronounced minimum in M_{lw} suggesting the occurrence of early morning thunderstorms. Midlevel cloud optical depth is the greatest overall with a mean value of ~12. Both the mean clear-sky and total albedos are nearly symmetrical about their noon values, of 0.16 and 0.25, respectively.

Figure 3 shows the average daytime cloud amounts for low, high, cirrus, midlevel, and high clouds. Cirrus clouds are defined as high clouds with $\tau < 6$. Mean cloud altitude is also given in Figure 3f. A southwest-to-northeast gradient in total cloudiness is evident in Figure 3e with values as low as 19% over west Texas and as large as 78% over southeastern Iowa. Low clouds (Figure 3a) are significant only in the southeastern quadrant of the domain with a maximum of 22%. Midlevel cloudiness (Figure 3d) is greatest over the northern portion of the domain, while high clouds (Figure 3b) account for more than half the cloudiness in eastern Missouri. Cirrus clouds (Figure 3c) are the major component of clouds over the southwest and the area slightly northwest of the SCF. Cirrus was observed over the SCF in 34% of the daytime measurements with a mean of 17% compared to 44% and 25% for all high clouds. The predominance of the cirrus clouds is evident in Figure 3f with the occurrence of the greatest mean cloud heights over the western and northeastern portions of the domain.

Total cloud optical depths (Figure 4a) follow the same gradient as total cloud fraction except for the small values of τ over Colorado. Mean cirrus optical depth in central Kansas and Oklahoma is close to 2 (Figure 4d). The smallest and greatest values are found over northeastern Texas and Missouri, respectively. The greater occurrence of high clouds and the larger total and cirrus optical depths over the northeastern quadrant suggest that much of the cirrus cloudiness may be generated by deep convective processes. The small mean values of M_{lw} (Figure 4b) and the maxima in α_{sw} (Figure 4e) over that quadrant are consistent with thick high cloudiness. Mean total albedo in the southwest is less than 0.24 compared to values around 0.39 in the northeast. LWCF (Figure 4c) follows the cloudiness gradient, ranging from 12 to 49 Wm^{-2} from the southwest to the northeastern portion of the domain. Likewise, SWCF (Figure 4f) shows the same trends but with almost twice the magnitude and the opposite sign. Net cloud forcing (not shown) varies from ~5 Wm^{-2} in the southwest to almost -45 Wm^{-2} over northeastern Missouri with a net cooling of ~ 20 Wm^{-2} by the clouds for this time period.

Discussion

The mean cloudiness over the SCF (44%) is approximately 21% less than the climatological April mean of 55% derived from surface observations (Warren et al., 1986) for a 5° region surrounding the SCF. The standard deviations for the spring seasonal mean is 3% cloud cover suggesting that cloudiness was well below normal during April 1996. The daytime mean total cloudiness is also roughly 20% less than that observed over the same 0.3° region during April 1994 (Minnis et al., 1995) further indicating that the skies were drier than normal over central Oklahoma. Although the diurnal cycle over the region is not usually so strong as that seen in Figure 2a, the minimum cloud cover, as determined from local climatological data (LCD) from Oklahoma City, frequently occurs between 2200 and 0300 LT. The Oklahoma City LCD also reveal that in April 1979, the diurnal range was at least 30%, with a maximum of more than 60% . The LBTM cloud amounts are underestimated at night because of the lack of contrast in the IR between low clouds and the surface. Thus, the diurnal range in Figure 2a is probably too large. Its true value may be closer to the 30% observed during 1979.

Low-level cloudiness was less than the seasonal mean from surface observations (Warren et al., 1986). The relative maxima in low cloudiness in Figure 2a are probably due to stratus in the morning and cumulus during the afternoon (Warren et al., 1986). Mean midlevel cloudiness during the day is comparable to the spring seasonal mean of 13% seen from the surface (Warren et al., 1986). The amount of high cloud cover during SUCCESS is less than the Warren et al. (1986) climatology for spring, but it constitutes approximately the same proportion of total cloudiness. Because of edge effects, some of the pixels containing high clouds are interpreted as midlevel or low clouds resulting in some underestimation of cirrus in the satellite results. When cirrus occur over low clouds they may be interpreted as midlevel clouds causing additional underestimation of mean cirrus amount. The fractional coverage by cirrus during SUCCESS is greater than that observed in the GOES data during April 1994 although the high cloud amounts were essentially the same over the central part of the domain during both time periods. The similarities in the high cloud amounts are probably due to a greater number of thick cumulonimbus

and anvil clouds occurring during April 1994. Although the earlier optical depths reported by Minnis et al. (1995) are underestimated due to a calibration error, they are nearly twice as large as those observed during SUCCESS. A relatively frequent occurrence of thunderstorms could account for the same high cloud fraction, reduced cirrus amount, and increased optical depths during April 1994 compared to the SUCCESS period.

The difference in cloud amounts and types between April 1994 and 1996 is also evident in the albedos and LW fluxes. The corrected calibration for 1994 yields clear-sky albedos that are nearly identical to those in Figure 2c but total albedos are that are almost 20% greater. The April 1994 LW fluxes are also significantly lower than those in Figure 2d consistent with thicker high clouds during April 1994. The diminished cloudiness during SUCCESS probably affected T_{cs}. Over the SCF, for example, the daytime values of T_{cs} are ~ 8K greater than their April 1994 counterparts. The 24-hour surface air temperatures at the SCF were only 4 K greater during April 1996. While more detailed spatially, the magnitude and sign of the cloud forcing parameters are similar to those observed by Ramanathan et al. (1989) for April 1985.

Concluding Remarks

The results presented here indicate that April 1996 was an excellent time to conduct SUCCESS because of the abundance of cirrus clouds. As revealed in other papers from this issue, the variety of cirrus clouds was also substantial. In general, the period was unusually deficient in cloudiness with few deep convective events. Much of the heavier cloud cover was confined to the northeastern portion of the domain. The data can be accessed electronically at http://albedo.larc.nasa.gov:1123/arm.html. Comparisons of these results with other SUCCESS datasets will help determine the uncertainties in the cloud and radiation parameters. In general, the results show consistency between cloud properties and radiation fields indicating that the values are reasonably accurate. The high temporal and spatial variability and frequent occurrence of cirrus clouds should make the data from the SUCCESS period extremely valuable for testing cirrus process models.

Acknowledgments. David Doelling of AS&M, Inc. produced the narrowband-broadband conversions, while Louis Nguyen of AS&M, Inc. provided invaluable assistance in collecting and reducing the GOES data. This research was supported by the NASA Subsonic Assessment Program and First ISCCP Regional Experiment Program through NASA/Office of Mission to Planet Earth and by the Department of Energy Environmental Sciences Division, Inter Agency Transfer Agreement (ITF#21422116AQ) through Pacific Northwest Laboratories and Inter Agency Agreement #DE-AI02-97ER62341 as part of the Atmospheric Radiation Measurement Program.

References

Minnis, P., K. N. Liou, and Y. Takano, Inference of cirrus cloud properties using satellite-observed visible and infrared radiances. Part I: Parameterization of radiance fields. *J. Atmos. Sci.*, **50**, 1279-1304, 1993.

Minnis, P., W. L. Smith, Jr., D. P. Garber, J. K. Ayers, and D. R. Doelling, Cloud properties derived from GOES-7 for the Spring 1994 ARM Intensive Observing Period using version 1.0.0 of the ARM satellite data analysis program. *NASA RP 1366*, August, 59 pp., 1995.

Minnis, P., J. K. Ayers, L. Nguyen, W. L. Smith, Jr., and R. Palikonda, Calibration of satellite visible and infrared sensors for field experiments and the ARM Program. Submitted to *J. Atmos. Oceanic Tech.*, 1997a.

Minnis, P., D. R. Doelling, F. P. J. Valero, S. Pope, Validation of narrowband-derived broadband shortwave albedos and longwave fluxes using ARESE and SCARAB flux datasets. Submitted to *J. Geophys. Res.*, 1997b.

Ramanathan, V., R. D. Cess, E. F. Harrison, P. Minnis, B. R. Barkstrom, E. Ahmad, and D. Hartmann, Cloud-radiative forcing and climate: results from the Earth Radiation Budget Experiment. *Science*, **243**, 57-63, 1989.

Warren, S. G., C. J. Hahn, J. London, R. M. Chervin, and R. L. Jenne, Global distribution of total cloud amounts and cloud type amounts over land. NCAR/TN-273 + STR, 229 pp., 1986.

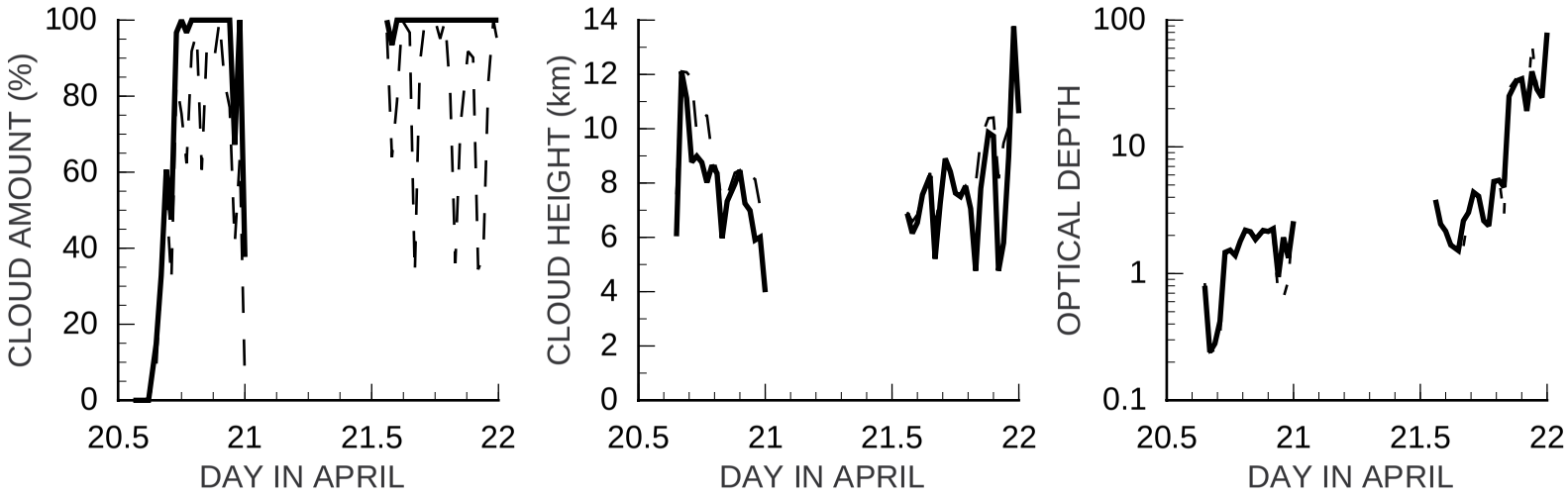

Figure 1. Daytime total (solid) and high (dashed) cloud properties for April 20-21, 1996 over the ARM SCF.

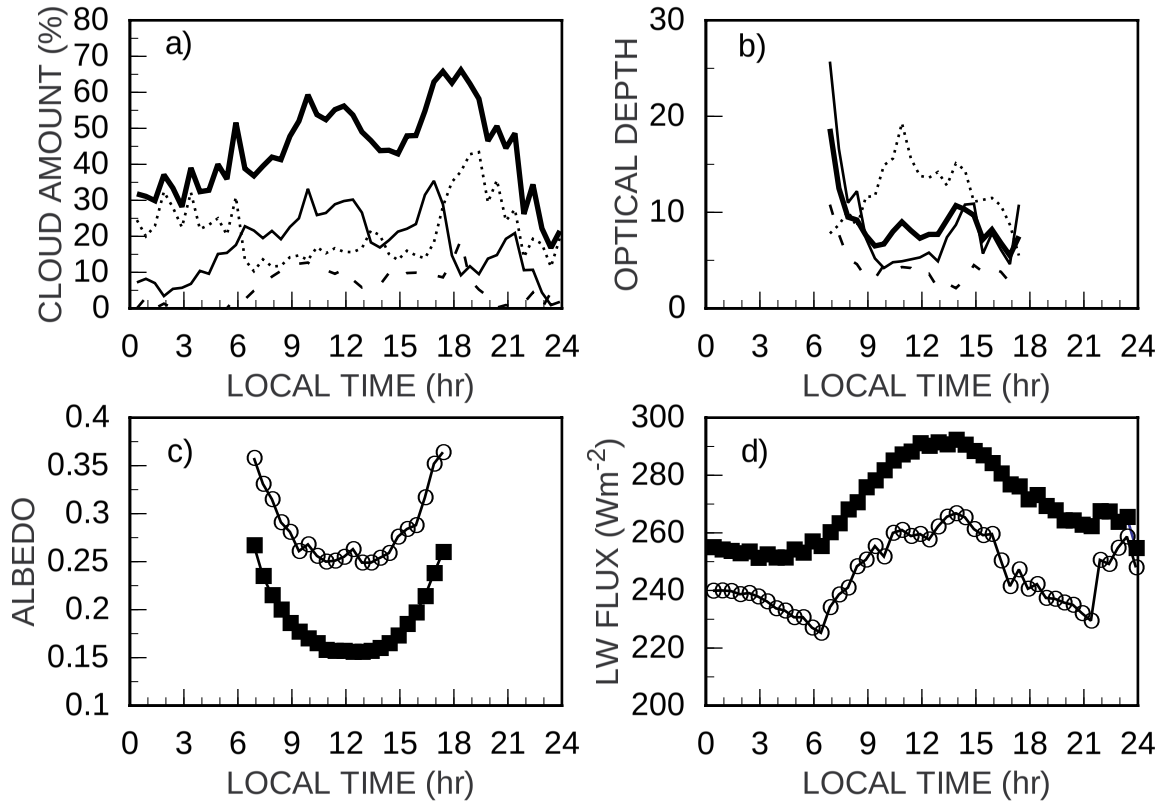

Figure 2. Mean diurnal variation of cloud and radiative parameters over SCF 0.3° box during SUCCESS (April 9 - May 9, 1995) for low (dotted), midlevel (long dash), high (thin solid), and total (heavy solid) clouds and clear (solid symbols) and total (open symbols) albedo and LW flux.

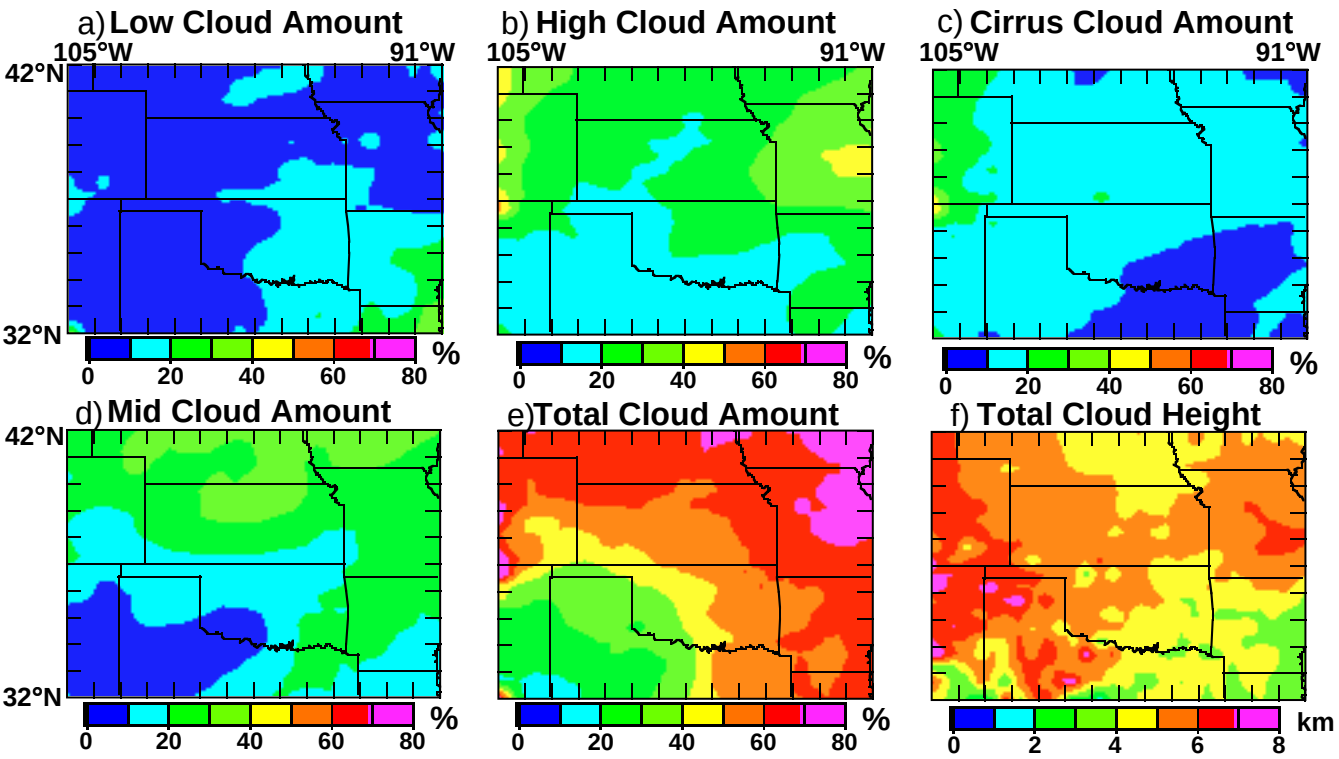

Figure 3. Mean daytime cloud properties derived from GOES-8 during SUCCESS, April 9 - May 9, 1996.

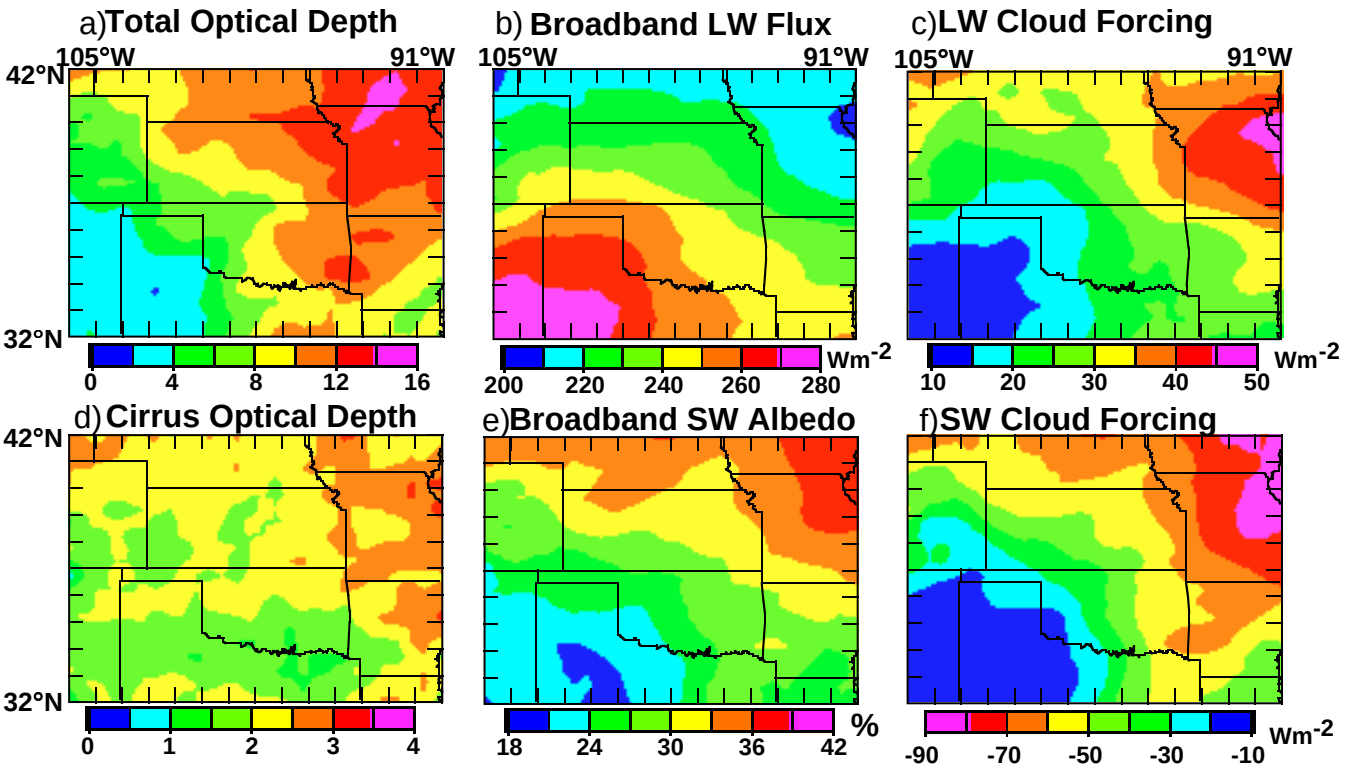

Figure 4. Same as Figure 3, except for radiative properties. Cloud forcing and LW flux for 24 hours.